# Magnetic and structural anisotropies of Co_2FeAl Heusler alloy epitaxial thin films

M. S. Gabor, T. Petrisor, C. Tiusan, Michel Hehn, T. Petrisor

# Magnetic and structural anisotropies of $Co_2FeAl$ Heusler alloy epitaxial thin films

M. S. Gabor, T. Petrisor Jr., and C. Tiusan*
*Materials Science Laboratory, Technical University of Cluj-Napoca, Cluj-Napoca, Romania and*
*Institut Jean Lamour, Département P2M, Centre National de la Recherche Scientifique, Nancy University, Nancy, France*

M. Hehn
*Institut Jean Lamour, Département P2M, Centre National de la Recherche Scientifique, Nancy University, Nancy, France*

T. Petrisor
*Materials Science Laboratory, Technical University of Cluj-Napoca, Cluj-Napoca, Romania*
(Received 21 February 2011; published 12 October 2011)

This paper shows the correlation between chemical order, lattice strains, and magnetic properties of Heusler $Co_2FeAl$ films epitaxially grown on MgO(001). A detailed magnetic characterization is performed using vector-field magnetometery combined with a numerical Stoner-Wohlfarth analysis. We demonstrate the presence of three types of in-plane anisotropies: one biaxial, as expected for the cubic symmetry, and two uniaxial. The three anisotropies show different behavior with the annealing temperature. The biaxial anisotropy shows a monotonic increase. The uniaxial anisotropy that is parallel to the hard biaxial axes (related to chemical homogeneity) decreases, while the anisotropy that is supposed to have a magnetostatic origin remains constant.

DOI: 10.1103/PhysRevB.84.134413 PACS number(s): 85.75.−d, 75.70.Ak, 75.30.Gw, 75.47.Np

## I. INTRODUCTION

Half-metallic ferromagnets (HMFs) represent alternative candidates for magnetic electrodes in magnetic tunnel junctions and current-perpendicular-to-plane (CPP) spin valves. Since they have an energy gap around the Fermi level $E_F$ in the minority spin band, theoretically, they are expected to provide 100% spin polarization. Among the HMFs, a special class is represented by the full-Heusler alloys. These compounds are described by the formula $X_2YZ$, where $X$ and $Y$ are transition metals and $Z$ is a main group $sp$ element. Recent theoretical predictions[1,2] indicate that the Co-based full-Heusler alloys should behave like half-metals even at room temperature. Presently, one of the most studied full-Heusler alloys is $Co_2FeAl$ (CFA). It was demonstrated to provide giant tunneling magnetoresistance (GTMR) effects in magnetic tunnel junctions[3,4] and has a low Gilbert damping.[5] While the low damping is essential for spin switching with low currents and spin torque oscillators, it enhances the spin-torque-induced mag noise in CPP giant magnetoresistance (GMR) sensors. This is one of several reasons why CPP GMR sensors are not yet competitive.

However, the integration of CFA as a ferromagnetic electrode in spintronic devices requires a precise knowledge and control of its magnetic properties. In this sense, one of the key parameters is the magnetic anisotropy, which should be large for magnetic storage and low for magnetic switching applications. Fundamentally, the magnetic anisotropy is directly related to the spin-orbit-coupling relativistic effect. Therefore, modifications of the electronic structure in bulk, surface, or interfaces are expected to lead to important changes in the magnetic anisotropy.[6,7]

The crystalline structure of Heusler alloys is cubic, belonging to the $Fm\bar{3}m$ space group. Therefore, the (001) epitaxial films are expected to show an in-plane fourfold magnetic anisotropy. However, for the case of Heusler alloys grown on GaAs(001) substrates,[8–14] a dominant in-plane uniaxial magnetic anisotropy (UMA) has often been reported. This uniaxial term can be reduced by buffering the GaAs substrate with MgO for $Co_2MnSi$ films,[13] whereas for $Co_2Cr_{0.4}Fe_{0.4}Al$ films[10] the MgO buffering has no major effect. Uniaxial anisotropy contributions have been also reported for Heusler films deposited on sapphire substrates,[15,16] Si(111),[17] Ge(111),[18] and MgO(001).[19–21] Moreover, extra UMAs have been reported not only for Heusler alloys but for different magnetic cubic crystal symmetry systems grown on various substrates.[7] The complex origin of this additional UMA is still under debate. Several mechanisms are evoked as possible causes: symmetry breaking at atomic-stepped substrates,[22–24] anisotropic strain relaxation,[25,26] film morphology,[27,28] and self-shadowing effects in oblique deposition.[29]

In this paper we report a detailed study on the structural and magnetic properties of CFA thin films epitaxially grown on MgO-buffered MgO(001) single-crystalline substrates. Our analysis demonstrates that a direct correlation exists between the in-plane magnetic anisotropy and the structural evolution of the CFA film, tuned by annealing. Moreover, we illustrate here that a magnetic analysis, dedicated to extract the different anisotropy terms of epitaxial CFA films, can be successfully performed within a Stoner-Wohlfarth coherent rotation model, which includes a biaxial and two uniaxial anisotropy contributions.

## II. EXPERIMENT

The CFA films are grown on MgO-buffered MgO(001) single-crystal substrates using rf magnetron sputtering. The base pressure in the deposition chamber is lower than $3 \times 10^{-8}$ Torr. Prior to deposition the substrates are degassed *in situ* at 600 °C. Then a 10-nm-thick MgO-buffer layer is deposited at room temperature by rf sputtering from a MgO polycrystalline target under an Ar pressure of 5.0 mTorr. The MgO layer improves the flatness quality of the substrate and traps the residual carbon, thus preventing further diffusion across the

 

stack during subsequent annealing stages. After the buffer-layer deposition, a 55-nm-thick CFA film is sputtered at room temperature in rf plasma from a stoichiometric target ($Co_{50\%}Fe_{25\%}Al_{25\%}$) under 1.0 mTorr of Ar. Finally, the films are capped with 5 nm of MgO. After the growth of the stack, the films are flash annealed for 10 min in a vacuum lower than $3 \times 10^{-8}$ Torr at 400, 500, and 600 °C.

The structural properties of the samples have been analyzed by x-ray diffraction (XRD) using a high-resolution four-circle diffractometer. The magnetic characteristics were investigated by vibrating sample magnetometry equipped with a vector-field characterization option.

## III. RESULTS AND DISCUSSION

### A. Structural properties

Figure 1 shows x-ray $2\theta$-$\omega$ (out-of-plane) diffraction patterns for MgO-buffered CFA films as deposited and annealed at 400, 500, and 600 °C. An analysis of the XRD patterns illustrates that in addition to the peak corresponding to the MgO substrate, all the samples exhibit only the (002) and (004) peaks of the CFA. Theoretically, in terms of the chemical order, the CFA crystal may be in a perfectly chemically ordered $L2_1$ phase, a $B2$ phase characterized by total disorder between Fe and Al while Co atoms occupy regular sites, and the $A2$ phase, which is totally disordered with respect to Fe, Al, and Co. In our samples, the presence of the (002) CFA reflection indicates that the films contain the $B2$ phase. The perfectly ordered $L2_1$ structure would be characterized by the presence of superlattice reflections such as (111) or (311).[30] In order to test the occurrence of superlattice peaks we perform in-plane $\phi$ scan measurements. Within the accuracy of the measurements, no $L2_1$-type reflections could be observed. This suggests that in our samples the $B2$ structural phase dominates. Polar figures (not shown here) confirm the epitaxial growth of the CFA films

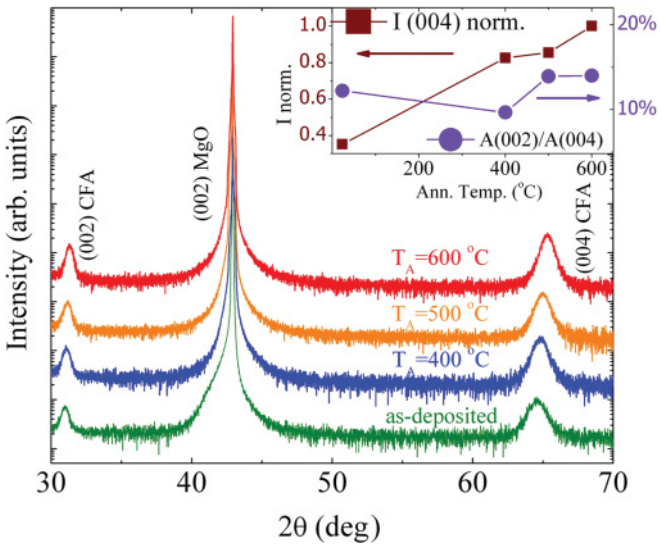


FIG. 1. (Color online) X-ray $2\theta$-$\omega$ diffraction pattern for the MgO-buffered CFA films as a function of annealing temperature. The inset shows the evolution of the CFA(004) peak normalized intensity $I(004)$ and the ratio of the integral intensities of the (002) and (004) CFA peaks $A(002)/A(004)$ with respect to the annealing temperature.

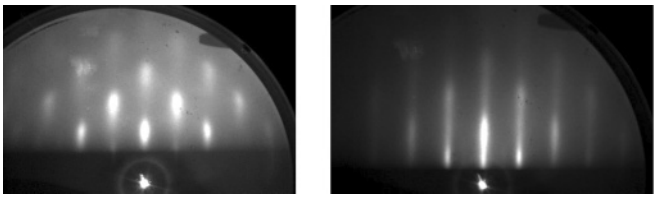

FIG. 2. Reflection high-energy electron-diffraction patterns recorded for samples, as deposited (left-hand side) and annealed at 600 °C (right-hand side), showing the improvement of the crystallographic quality with annealing.

according to the expected CFA(001)[110]‖MgO(001)[100] epitaxial relation.

The inset in Fig. 1 shows the evolution of the normalized intensity $I(004)$ of the (004) CFA reflection versus the annealing temperature. The normalized intensity shows a monotonic increase with the annealing temperature, with a significant jump for the sample annealed at 400 °C relative to the as-deposited sample. This implies an important improvement of the structure at the atomic level for the annealed samples. It is reasonable to assume that the as-deposited samples contain regions with structural or crystalline disorder that vanishes upon annealing. This represents a transition from short-range to long-range crystallographic order. Reflection high-energy electron-diffraction analysis, performed on similar samples transferred and annealed in an UHV chamber, supports this expectation and also indicates an overall improvement of the crystallization degree (see Fig. 2).

The (002) reflection is characteristic of the $B2$ structure. Thus the integrated peak intensity ratio $A(002)/A(004)$ represents a measure of the degree of order on Co sites. This ratio, shown in the inset of Fig. 1, exhibits a decrease for the 400 °C annealed sample, relative to the as-deposited sample, although the $I(004)$ intensity increases significantly. This may be related to the presence of regions with structural disorder in the as-deposited sample that, with annealing, crystallize in the chemically disordered $A2$ structure, thereby increasing $I(004)$ and reducing the $A(002)/A(004)$ ratio. As the annealing temperature increases further, the $A2$ phase gradually evolves toward the better chemically ordered $B2$ phase, thus leading to an increase of the $A(002)/A(004)$ ratio.

The in-plane $a_\parallel$ and out-of-plane $a_\perp$ lattice parameters of the epitaxial CFA films were determined by performing reciprocal lattice scans. First, we carried out an $l$ scan ($2\theta$-$\omega$ symmetrical geometry) around the (002) node of the CFA reciprocal lattice and obtained the $d_{002}$ distance, which allows us to calculate $a_\perp$. Using this $l$ coordinate, we performed an $h = k$ scan ($\omega$-$2\theta$ asymmetrical geometry) around the (224) CFA reciprocal lattice node and obtained the $d_{224}$ distance, which we used to derive $a_\parallel$. The obtained values are depicted in Fig. 3.

From Fig. 3 one can observe that the as-deposited film experiences a relatively strong tetragonal distortion. As the annealing temperature increases the distortion relaxes by formation of misfit dislocations. Periodic arrays of columnar misfit dislocations across the entire thickness of the CFA film have been observed on films annealed at 600 °C from phase analysis of cross-section transmission electron microscopy images (not presented here). The XRD investigation

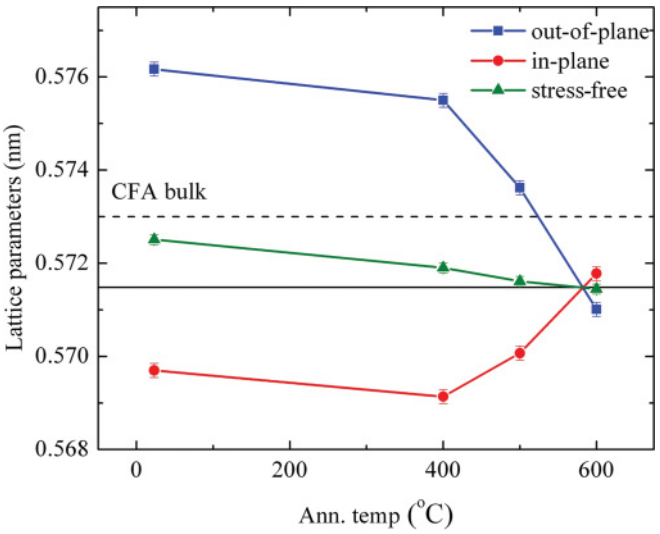


FIG. 3. (Color online) Evolution of the out-of-plane and in-plane lattice parameters versus the annealing temperature. The stress-free lattice parameter is also plotted. The dashed lines represents the bulk $L2_1$ ordered CFA lattice parameter. The horizontal solid line marks the position of the stress-free lattice parameter $a_0^{600}$ after annealing at 600 °C.

demonstrates that the lattice parameter after annealing is smaller than the bulk value of the perfectly ordered $L2_1$ cell. This could be explained by the presence of some $A2$-type disorder, as already reported in the literature.[31]

Our analysis illustrates a totally counterintuitive evolution of the lattice parameters with annealing. Due to the in-plane tensile stress between the film and the MgO buffer, one would expect the in-plane lattice parameter to be larger than the out-of-plane one and eventually the distortion to be relaxed with annealing by plastic relaxation (e.g., formation of misfit dislocations). The unusual lattice distortion is most likely connected to the growth method. As illustrated in the literature,[32] during the growth of films by sputtering, the bombardment of the film by energetic neutral atoms reflected off the target can create point defects in the lattice or regions with structural disorder. These will generate local strain fields that can disturb the crystallization and may give rise to lattice distortion such as that observed in our films.

To gain further insight into the strain evolution with the annealing temperature we have plotted in Fig. 3 the stress-free lattice parameter of CFA, calculated according to elasticity theory:

$$a_0 = \frac{C_{11}a_\perp + 2C_{12}a_\parallel}{C_{11} + C_{12}}, \qquad (1)$$

where $C_{11}$ and $C_{12}$ are the elastic stiffness constants. The stiffness constants were calculated using the elastic package implemented in the *ab initio* FPLAPW WIEN2K code.[33] In order to calculate the three independent elastic constants $C_{11}$, $C_{12}$, and $C_{44}$ three types of strains corresponding to highly symmetric types of deformation have been considered: isotropic deformation by varying the cubic volume, tetragonal volume-conserving distortion, and rhombohedral distortion. The total energy of the system is calculated *ab initio* for each distorted configuration and then fitted with polynomial models.

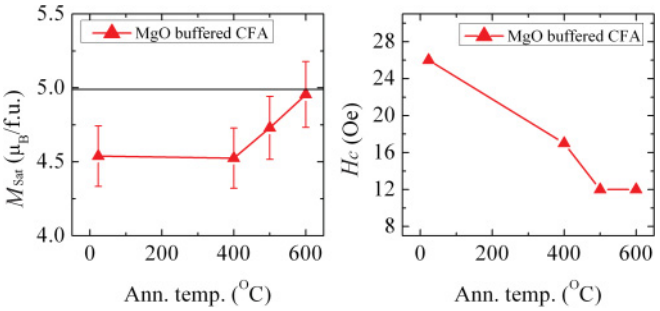


FIG. 4. (Color online) Evolution of the saturation magnetization and coercive field, measured along the easy axis, as a function of annealing temperature for MgO-buffered CFA films.

From this analysis one gets a set of equations allowing the determination of the full elastic tensor components. Using this formalism, we obtain the following values for the elastic constants: $C_{11} = 253$ GPa, $C_{12} = 165$ GPa, $C_{44} = 153$ GPa.

The theoretical temperature variation of the lattice parameter is calculated using the *ab initio* extracted values for the elastic constants and the experimental temperature variation for $a_\perp$ and $a_\parallel$. If one assumes only an elastic type of stress in the films, then if the in-plane lattice parameter changes, the out-of-plane parameter should change accordingly so that the stress-free lattice parameter remains constant. As can be seen in Fig. 3, the stress-free lattice parameter of the as-deposited film is increased by 0.2% with respect to the one corresponding to the 600 °C annealed film. The expansion progressively reduces with annealing once the crystallization and chemical order are enhanced. This verifies that for as-deposited and low-temperature annealed samples, there is stress related to crystallographic point defects, poorly crystalized regions, or even regions of different chemical order.

### B. Magnetic properties

In order to study the magnetic properties of our films, we perform hysteresis loops and angular remanence magnetization (ARM) measurements at room temperature with the magnetic field applied parallel to the film surface. Figure 4 shows the saturation magnetization $M_{sat}$ and coercive field $H_c$, measured along the [−110] crystallographic direction, as a function of annealing temperature. The saturation magnetization for the as-deposited and 400 °C annealed films has roughly the same value that for higher annealing temperatures evolves toward the theoretically predicted one.[1] This confirms that the structural evolution of the annealed samples from as-deposited to 400°C is not related to a significant stoichiometry variation (accompanied by a change in $M_{sat}$). This is most likely a crystallization-related effect. As supported by structural analysis (Sec. III A), the system practically evolves from a local (short-range) crystallographic order toward a long-range crystalline order. However, this transition from disordered toward a crystallographically ordered and chemically disordered $A2$ phase does not affect the magnetization. On average, within the regime of the chemical disorder, the total magnetic moment remains constant. An accurate quantitative temperature variation of $M_{sat}$ is difficult due to the large error bars (see Fig. 4). However, beyond 400 °C, the increase in $M_{sat}$ can be attributed to the improvement of the chemical order and

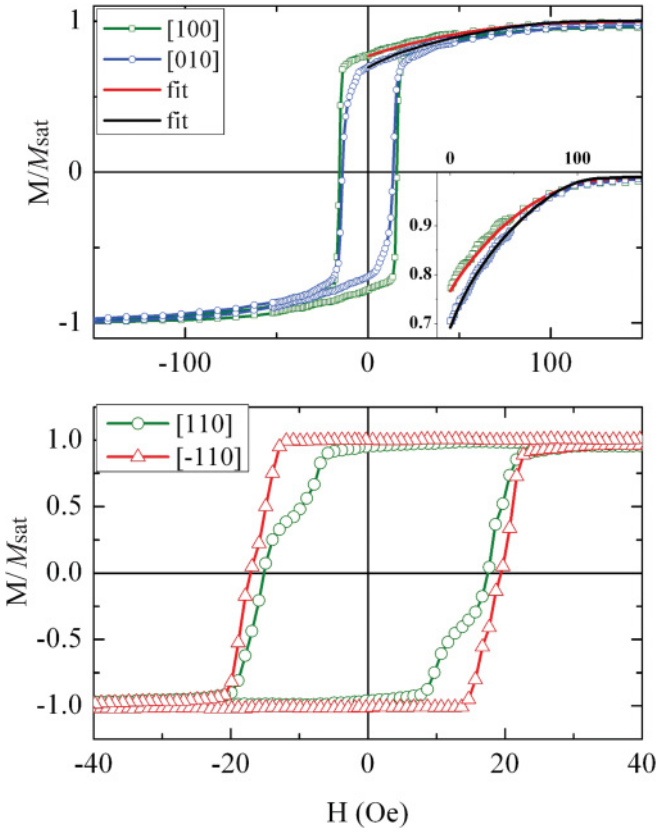


FIG. 5. (Color online) Magnetization loops along the main crystallographic axes for the film annealed at 400 °C. The inset shows a closeup of the data used for a numerical fitting and the result of the fit (solid lines).

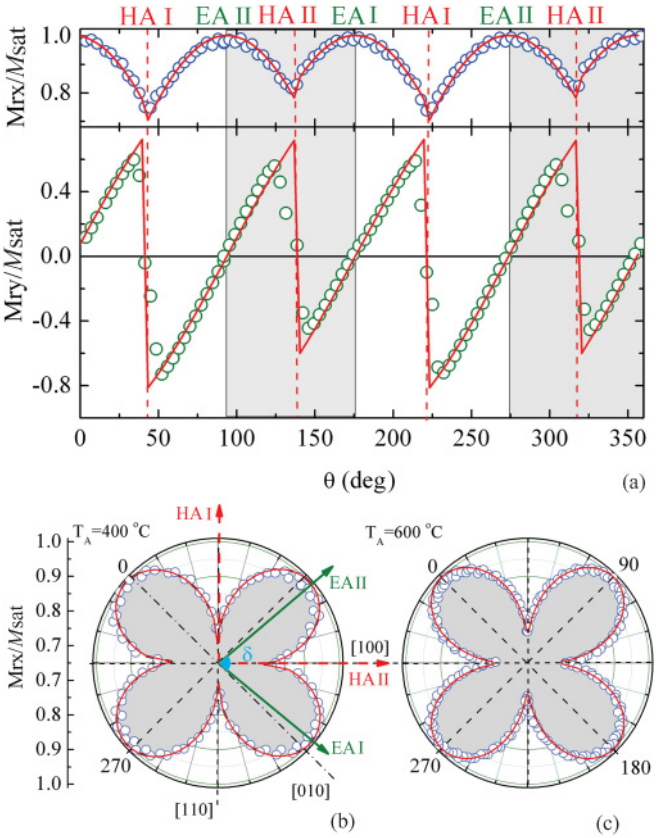


FIG. 6. (Color online) Angular remanence magnetization measurements for the sample annealed at (a) and (b) 400 °C and (c) 600 °C. The symbols represents experimental data while lines are numerical simulations according to the model described in the text. The positions of the overall easy and hard axes are also represented in (a).

local stoichiometry. This leads to a change in the saturation magnetization, as reflected by the curve plotted in Fig. 4. The decrease of $H_c$ with annealing is consistent with the reduction of the defect density with enhancing crystalline quality.

Magnetic hysteresis loops, recorded along the main crystallographic directions, are shown in Fig. 5 for the film deposited on the MgO-buffer layer and annealed at 400 °C. All samples show easy magnetization axes along the CFA [110] and [−110] crystallographic directions and hard axes parallel to [100] and [010]. Figure 5 shows that the two easy axes are not equivalent. Inequivalent hard axes are also shown. This leads us to conclude that for CFA films deposited on MgO, the biaxial anisotropy is altered by the superposition of two uniaxial in-plane anisotropies: one with the easy axis parallel to the [110] direction and the other with the easy axis parallel to the [100] direction.

To gain quantitative insight into the magnetic properties of the CFA films we perform numerical simulations based on the macrospin Stoner-Wohlfarth formalism.[34] We define a total-energy functional containing anisotropy energy terms related to one in-plane biaxial anisotropy and two in-plane uniaxial anisotropies rotated 45° with respect to each other:

$$E = \frac{K_4}{4}\sin^2(2\theta) + K_U^1 \sin^2\left(\theta + \frac{\pi}{4}\right) + K_U^2 \sin^2\left(\theta + \frac{\pi}{2}\right) - \mu_0 M_{\text{sat}} H \cos(\phi - \theta), \quad (2)$$

where $M_{\text{sat}}$ is the saturation magnetization, $H$ is the applied field, $\theta$ and $\phi$ are the angles of the magnetization and applied field relative to the easy axis direction (i.e., [110]), $K_4$ is the biaxial anisotropy constant, $K_U^1$ is the uniaxial anisotropy constant parallel to the biaxial hard axis, and $K_U^2$ is the uniaxial anisotropy constant parallel to the biaxial easy axis.

To determine the anisotropy constants for these samples we took up to four hysteresis loops, measured in the proximity of the hard axes, and fitted them simultaneously within the Stoner-Wohlfarth coherent rotation model, using as parameters the anisotropy constants. When fitting the hysteresis curves, we limited ourselves to the reversible part of the $M$-$H$ loop for which we can assume coherent rotation, i.e., from saturation toward zero applied field (see the inset of Fig. 5).

With the values obtained for the anisotropy constants we simulated the theoretical ARM curves. The results are illustrated in Fig. 6, which shows very good agreement between the experimental points and the simulations (solid lines).

For the 400 °C annealed sample the effect of UMA parallel to the biaxial hard axis is to rotate the overall easy axes at an angle $\delta$ other than 90° [Fig. 6(b)]. The effect of the UMA

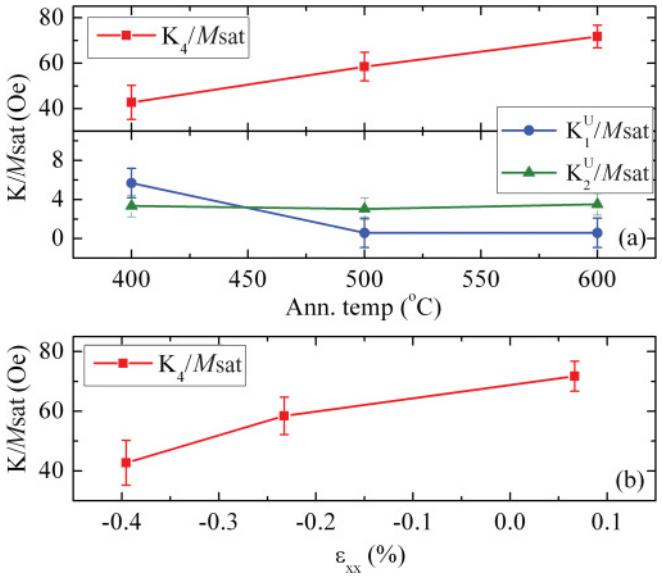


FIG. 7. (Color online) Evolution of the cubic $K_4/M_{sat}$ and uniaxial $K_U^1/M_{sat}$ and $K_U^2/M_{sat}$ anisotropy fields with annealing temperature for the samples deposited on MgO-buffered substrates (a) and the variation of the four-fold anisotropy field with the in-plane biaxial strain (b).

parallel to the biaxial easy axis is to increase the area of the lobes in the ARM polar plot. This can be easily verified in simulations by setting $K_U^2 = 0$. Figure 6(c) shows that for high enough annealing temperatures the effect of UMA parallel to the hard axis vanishes.

The values of the anisotropy fields deduced from the numerical fitting are shown in Fig. 7. The fourfold anisotropy field $K_4/M_{sat}$ increases with annealing, $K_U^1/M_{sat}$ decreases to negligible values for annealing temperatures above 400 °C, and $K_U^2/M_{sat}$ remains independent of the annealing temperature. It should be noted that in the case of the as-deposited sample, we were not able to fit the experimental magnetization curves within the framework of our simple model. This is most likely due to the complex crystallographic structure (higher degree of crystallographic disorder) observed for this sample, as mentioned in Sec. I.

One of the most interesting features reported in Fig. 7 is that the small-amplitude $K_U^2/M_{sat}$ remains practically independent of the annealing temperature. We suppose that this temperature-independent uniaxial anisotropy has a magnetostatic origin related to stepped substrates due to a small miscut[35] along the [100] substrate crystallographic direction corresponding to the [110] CFA one. To verify this assumption, we built samples using a 20-nm-thick Cr-buffer layer. In these samples the substrate morphology influence is expected to vanish. Indeed, for these Cr-buffered samples we did not observed any UMA parallel to the biaxial anisotropy easy axes (the two fourfold easy axes being equivalent). A figure of merit of our analysis model is the capability of extracting with accuracy small anisotropy constants and showing their invariance with the temperature.

To elucidate the origin of the UMA parallel to the biaxial hard axes we performed an extensive XRD analysis. However, within the accuracy of the XRD measurements we could not confirm any correlation between the UMA and possible in-plane structural anisotropy or anisotropic strain relaxation. By increasing the annealing temperature from 400 to 500 °C the UMA practically vanishes. The only difference between the sample annealed at 400 °C and the one annealed at 500 °C is the degree of chemical ordering (see Fig. 1). Therefore, we argue that this UMA is the result of an anisotropic chemical disorder in the films. The presence of chemically disordered domains, separated irregularly along the MgO [110] and MgO [1−10] crystallographic axes and vanishing for high annealing temperatures (>550 °C) was already identified[36] using low-energy electron diffraction in the case of the related $Co_2Cr_{0.6}Fe_{0.4}Al$ Heusler compound grown on MgO(001). This result is in agreement with and comes to further support our conclusion that the uniaxial magnetic anisotropy is a result of an anisotropic chemical disorder in the films. At this point we have no clear explanation why the favored direction of this UMA easy axis is [100] as opposed to [010]. Further explanation would require identifying some symmetry-breaking mechanism, for example, the miscut of the substrate.

One can see from Fig. 7 that $K_4/M_{sat}$ increases continuously with annealing. The origin of this increase could be correlated with the improvement of the chemical order within the cubic symmetry of the CFA films with annealing, as confirmed by the decrease of the uniaxial $K_1^U/M_{sat}$. However, at annealing temperatures above 500 °C, $K_1^U/M_{sat}$ is practically zero, whereas $K_4/M_{sat}$ continues to increase. Therefore, an additional mechanism for the temperature dependence of the biaxial anisotropy has to be considered. It is related to the evolution in temperature of the in-plane biaxial strain $\varepsilon_{xx} = (a_\parallel - a_0^{600})/a_0^{600}$. The biaxial anisotropy constant is connected to the in-plane biaxial strain through the magnetoelastic coupling parameters.[37] We are unaware of any reports in the literature estimating the values of these constants. This would have allowed us to quantify and extract precisely the strain contribution to the total variation of $K_4/M_{sat}$ with the annealing temperature. However, in Fig. 7(b) we plot the biaxial anisotropy constant, extracted from magnetic analysis, as a function of the in-plane biaxial strain, extracted from x-ray measurements. This confirms a direct correlation between fourfold anisotropy and biaxial strain, without being able to discriminate between the relative ratio of the strain and the chemical order contributions.

Our analysis provides values for the anisotropy constants, especially for the biaxial anisotropy, which are in good agreement with the ones reported in the literature for related $Co_2MZ$ Heusler compounds (for a list of available data see Ref. 38). Moreover, a complex study by Trudel *et al.*[21] illustrates the presence and evolution with annealing of biaxial and uniaxial anisotropies in $Co_2Fe_{0.5}Al_{0.5}Si$ grown on MgO(001). Our data are in good qualitative agreement with the results reported by Trudel *et al.*, with quantitative differences being related only to electronic structure direct effects in our $Co_2FeAl$ samples without Si substitutions and to the difference in the ordering degree of our $Co_2FeAl$ (only $B2$) with respect to their $Co_2Fe_{0.5}Al_{0.5}Si$ ($B2$ evolution toward $L2_1$).

## IV. CONCLUSION

In this paper we presented a detailed structural and magnetic analysis of CFA thin films epitaxially grown on MgO(001) substrates. The evolution of the chemical order and the lattice parameters with the annealing temperature has been studied. An exhaustive magnetic characterization of the CFA films has been performed using vector-field vibrating sample magnetometery combined with a numerical Stoner-Wohlfarth analysis. This allowed us to demonstrate the presence of three types of in-plane anisotropies: biaxial (as expected for the cubic symmetry) and two uniaxial contributions parallel to the biaxial easy and hard axes. The biaxial anisotropy shows a monotonic increase with the annealing. The uniaxial anisotropy related to chemical order decreases while the other, which is thought to have magnetostatic origin, remains constant with the annealing. These behaviors have been correlated with the chemical homogeneity and strain evolution within the films.

## ACKNOWLEDGMENTS

This work was partially supported by CNCSIS UEFISCSU, Projects No. PNII IDEI 4/2010, code ID-106 and No. POS CCE ID.574, code SMIS-CSNR 12467. C.T. acknowledges SPINCHAT Project No. ANR- 07-BLAN-341.

*coriolan.tiusan@phys.utcluj.ro

[1] I. Galanakis, P. H. Dederichs, and N. Papanikolaou, Phys. Rev. B **66**, 174429 (2002).
[2] S. Picozzi, A. Continenza, and A. J. Freeman, Phys. Rev. B **66**, 094421 (2002).
[3] W. Wang, H. Sukegawa, R. Shan, S. Mitani, and K. Inomata, Appl. Phys. Lett. **95**, 182502 (2009).
[4] W. Wang, E. Liu, M. Kodzuka, H. Sukegawa, M. Wojcik, E. Jedryka, G. H. Wu, K. Inomata, S. Mitani, and K. Hono, Phys. Rev. B **81**, 140402 (2010).
[5] S. Mizukami, D. Watanabe, M. Oogane, Y. Ando, Y. Miura, M. Shirai, and T. Miyazaki, J. Appl. Phys. **105**, 07D306 (2009).
[6] D. Sander, Rep. Prog. Phys. **62**, 809 (1999).
[7] C. A. F. Vaz, J. A. C. Bland, and G. Lauhoff, Rep. Prog. Phys. **71**, 056501 (2008).
[8] T. Ambrose, J. J. Krebs, and G. A. Prinz, Appl. Phys. Lett. **76**, 3280 (2000).
[9] F. Y. Yang, C. H. Shang, C. L. Chien, T. Ambrose, J. J. Krebs, G. A. Prinz, V. I. Nikitenko, V. S. Gornakov, A. J. Shapiro, and R. D. Shull, Phys. Rev. B **65**, 174410 (2002).
[10] T. Yano, T. Uemura, K.-I. Matsuda, and M. Yamamoto, J. Appl. Phys. **101**, 063904 (2007).
[11] A. Hirohata, H. Kurebayashi, S. Okamura, M. Kikuchi, T. Masaki, T. Nozaki, N. Tezuka, and K. Inomata, J. Appl. Phys. **97**, 103714 (2005).
[12] M. Hashimoto, J. Herfort, H.-P. Schönherr, and K. H. Ploog, J. Appl. Phys. **98**, 104902 (2005).
[13] S. Kawagishi, T. Uemura, Y. Imai, K.-I. Matsuda, and M. Yamamoto, J. Appl. Phys. **103**, 07A703 (2008).
[14] W. H. Wang, M. Przybylski, W. Kuch, L. I. Chelaru, J. Wang, Y. F. Lu, J. Barthel, H. L. Meyerheim, and J. Kirschner, Phys. Rev. B **71**, 144416 (2005).
[15] H. Schneider, Ch. Herbort, H. Jakob, S. Wurmehl, and C. Felser, J. Phys. D: Appl. Phys. **40**, 1548 (2007).
[16] M. Belmeguenai, F. Zighem, T. Chauveau, D. Faurie, Y. Roussigné, S. M. Chérif, P. Moch, K. Westerholt, and P. Monod, J. Appl. Phys. **108**, 063926 (2010).
[17] S. Yamada, K. Hamaya, K. Yamamoto, T. Murakami, K. Mibu, and M. Miyao, Appl. Phys. Lett. **96**, 082511 (2010).
[18] K. Kasahara, K. Yamamoto, S. Yamada, T. Murakami, K. Hamaya, K. Mibu, and M. Miyao, J. Appl. Phys. **107**, 09B105 (2010).
[19] W. Wang, H. Sukegawa, R. Shan, T. Furubayashi, and K. Inomata, Appl. Phys. Lett. **92**, 221912 (2008).
[20] S. Trudel, J. Hamrle, B. Hillebrands, T. Taira, and M. Yamamoto, J. Appl. Phys. **107**, 043912 (2010).
[21] S. Trudel, G. Wolf, J. Hamrle, B. Hillebrands, P. Klaer, M. Kallmayer, H.-J. Elmers, H. Sukegawa, W. Wang, and K. Inomata, Phys. Rev. B **83**, 104412 (2011).
[22] R. K. Kawakami, E. J. Escorcia-Aparicio, and Z. Q. Qiu, Phys. Rev. Lett. **77**, 2570 (1996).
[23] M. Mathews, F. M. Postma, J. C. Lodder, R. Jansen, G. Rijnders, and D. H. A. Blank, Appl. Phys. Lett. **87**, 242507 (2005).
[24] J. Chen and J. L. Erskine, Phys. Rev. Lett. **68**, 1212 (1992).
[25] Y. B. Xu, D. J. Freeland, M. Tselepi, and J. A. C. Bland, Phys. Rev. B **62**, 1167 (2000).
[26] O. Thomas, Q. Shen, P. Schieffer, N. Tournerie, and B. Lépine, Phys. Rev. Lett. **90**, 017205 (2003).
[27] R. Moroni, D. Sekiba, F. Buatier de Mongeot, G. Gonella, C. Boragno, L. Mattera, and U. Valbusa, Phys. Rev. Lett. **91**, 167207 (2003).
[28] Q.-F. Zhan, S. Vandezande, C. V. Haesendonck, and K. Temst, Appl. Phys. Lett. **91**, 122510 (2007).
[29] L. Abelmann and C. Lodder, Thin Solid Films **305**, 1 (1997).
[30] D. Fruchart, R. Fruchart, Ph. L'Héritier, K. Kanematsu, R. Madar, S. Misawa, Y. Nakamura, P. J. Ziebeck, and K. R. A. Webster, in *Magnetic Properties of Metals*, edited by H. P. J. Wijn, Landolt-Börnstein, New Series, Group III, Vol. 19c, Pt. 2 (Springer-Verlag, Berlin, 1986).
[31] K. Inomata, S. Okamura, A. Miyazaki, M. Kikuchi, N. Tezuka, M. Wojcik, and E. Jedryka, J. Phys. D: Appl. Phys. **39**, 816 (2006).
[32] Y. Huttel, J. I. Cerdá, J. L. Martínez, and A. Cebollada, Phys. Rev. B **76**, 195451 (2007).
[33] P. Blaha, K. Schwarz, G. K. H. Madsen, D. Kvasnicka, and J. Luitz, *Wien2k, An Augmented Plane Wave Local Orbitals Program for Calculating Crystal Properties*, edited by K. Schwartz (Technical University of Wien, Wien, 2001).
[34] E. C. Stoner and E. P. Wohlfarth, Philos. Trans. R. Soc. London A **240**, 599 (1948).
[35] A. Encinas-Oropesa and F. N. V. Dau, J. Magn. Magn. Mater. **256**, 301 (2003).
[36] J.-P. Wüstenberg, J. Fischer, C. Herbort, M. Jourdan, M. Aeschlimann, and M. Cinchetti, J. Phys. D **42**, 084016 (2009).
[37] P. Bertoncini, P. Wetzel, D. Berling, A. Mehdaoui, B. Loegel, G. Gewinner, R. Poinsot, and V. Pierron-Bohnes, J. Magn. Magn. Mater. **237**, 191 (2001).
[38] S. Trudel, O. Gaier, J. Hamrle, and B. Hillebrands, J. Phys. D **43**, 193001 (2010).